Patterns in 3D Vertically Oscillated Granular Layers: Simulation and Experiment

C. Bizon,* M. D. Shattuck, J. B. Swift, W. D. McCormick, and Harry L. Swinney†

Center for Nonlinear Dynamics and Department of Physics, University of Texas, Austin, Texas 78712

(Received 13 June 1997; revised manuscript received 15 September 1997)

Numerical simulations and laboratory experiments are conducted for thin layers of particles in a vertically oscillated container as a function of the frequency f, amplitude A, and depth H. The same standing wave patterns (stripes, squares, or hexagons oscillating at $f/2$ or $f/4$) and wavelengths are obtained in the simulations and experiments for a wide range of (f, A) and two layer depths. Two model parameters are determined by fits at just two points (f, A, H). Simulation results lead to heuristic arguments for the onset of patterns and the crossover from squares to stripes. [S0031-9007(97)04971-5]

PACS numbers: 46.10.+z, 47.54.+r, 83.10.Pp, 83.70.Fn

Spatial patterns are often observed in systems driven away from thermal equilibrium [1]; a thin layer of vertically oscillated granular material constitutes such a pattern forming system [2,3]. For granular media, continuum equations analogous to the Navier-Stokes equations for fluids are not known; hence many of the methods that have been applied to the study of other pattern forming systems cannot yet be applied to granular media. While phenomenological models may be constructed [4], their connection to the real system must remain unclear until the physics of granular media is understood at a more microscopic level. This state of affairs has driven modelers to simulate directly the motions and interactions of large collections of particles [5,6]. However, these simulations have been limited to two dimensions (2D), where the variety of spatial patterns is absent.

We report on the first 3D simulations of patterns in vertically oscillated granular media. In our simulations and experiments, we consider layers of P particles of average diameter D in an evacuated square container of side length $L = 100D$. The container is oscillated sinusoidally in the vertical direction with frequency f and amplitude A. The layer depth H is defined by $H = P(\pi/6)(D^3/L^2)/\phi$, where the packing fraction ϕ was experimentally measured to be 0.58. We express the depth nondimensionally as $N = H/D$. We set P in our experiments and simulations to either 30 000 or 60 000, so that our layers have depth $N = 2.71$ or $N = 5.42$. We nondimensionalize the frequency and acceleration amplitude using the acceleration due to gravity g and the layer depth H [7]: $f^* = f\sqrt{H/g}$ (varied here in the range $0.1 < f^* < 2$) and $\Gamma = 4\pi^2 f^2 A/g$ (varied in the range $2 \leq \Gamma \leq 7$). In the simulations the particle diameters are distributed uniformly between $0.99D$ and $1.01D$; in most experiments we use lead particles sieved between 0.5 and 0.6 mm. The laboratory system is otherwise like that described in [3].

Our results from simulation and experiment are remarkably similar over the entire range of (f^*, Γ) examined, as Fig. 1 illustrates, with patterns obtained at seven values of (f^*, Γ). We will first discuss the simulations and then we will compare the wavelengths and patterns obtained in simulation and experiment.

Simulations.—In our event driven algorithm, particles interact only through instantaneous binary collisions and move only under the influence of gravity between collisions. Linear and angular momentum are conserved in collisions, while energy is dissipated. The interaction between particles is described by the coefficient of restitution e, the coefficient of sliding friction μ, and the rotational coefficient of restitution β; we will discuss each parameter in turn.

The value of the relative normal velocity v_n of colliding particles after a collision is calculated by multiplying the precollision value of v_n by $-e(v_n)$. The precise functional form of $e(v_n)$ is unknown, but measurements show that $e(v_n)$ decreases from unity as v_n increases from zero [8]. The simplest models use a constant e, but this disagrees with experiment and also leads to inelastic collapse, in which particles undergo an infinite number of collisions within a finite amount of time [9]. We assume that $e(v_n) = 1 - Bv_n^\alpha$ for v_n less than a crossover velocity v_0, and $e(v_n) = \epsilon$ for $v_n > v_0$, where $B = (1 - \epsilon)(v_0)^{-\alpha}$ and ϵ is a constant. The increase in e for low v_n avoids inelastic collapse [6,9], while constant e at higher v_n is more computationally efficient. The precise way in which e decreases from unity to ϵ is unimportant. Simulations for $\alpha = 0.5, 0.75$, and 1.0 yield the same patterns and wavelengths; in the present study we arbitrarily choose $\alpha = 0.75$. Similarly, simulations for $v_0 = \sqrt{gD}/3$, $\sqrt{gD}$, and $3\sqrt{gD}$ yield the same patterns and wavelengths; we use $v_0 = \sqrt{gD}$. This does not imply that material properties are dependent upon g or D, simply that the unit of velocity for our simulation is $\sqrt{gD}$.

The tangential component of the particle collisions is modeled with the collision operator in Ref. [10]. Angular momentum is conserved, and the tangential impulse is given by a coefficient of friction μ times the normal impulse. A cutoff is then imposed, corresponding to the

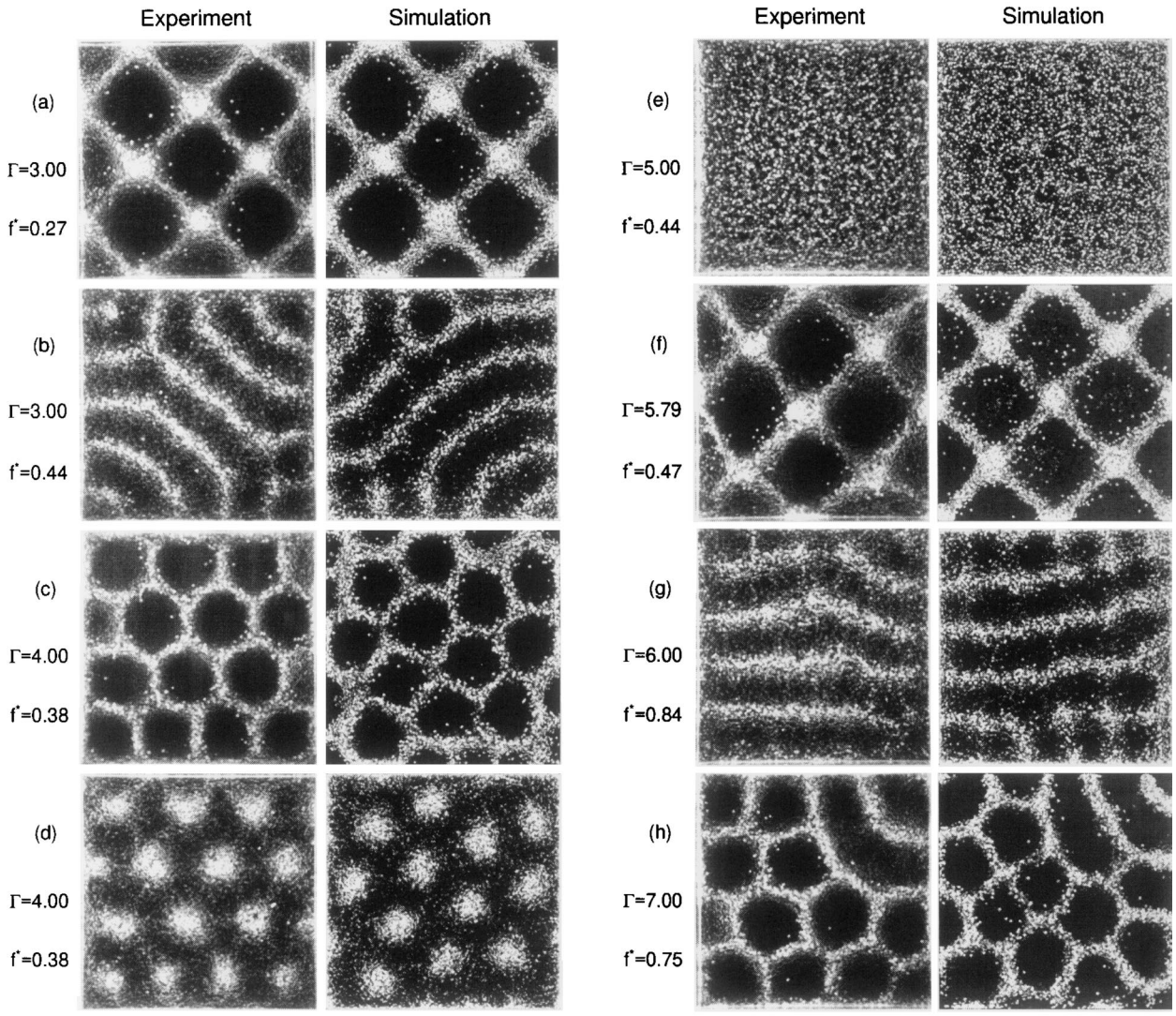

FIG. 1. Standing wave patterns: (a) squares, (b) stripes, (c) and (d) alternating phases of hexagons, (e) flat layer, (f) squares, (g) stripes, and (h) hexagons. Patterns (a)–(e) oscillate at f/2, (f)–(h) at $f/4$. The dimensionless layer depth N is 5.42. The brightness indicates the height of the layer. The experiments use lead spheres sieved between 0.5 and 0.6 mm.

crossover from a sliding contact to a rolling contact: the ratio of the relative surface velocity after the collision to that before the collision must always be greater than $-\beta_0$; we use $\beta_0 = 0.35$, as suggested in [10] based on comparison to experiments [11].

The collision operator is incorporated into an event driven simulation [12]. From known particle positions and velocities, the times at which given pairs of particles will collide are calculated. Time advances from one collision to the next, rather than with an externally imposed time step as in soft-sphere molecular dynamics algorithms. We use a delayed states algorithm [13] in which only the particles that collide are updated on a given time step. The efficiency of this algorithm allows us to perform all simulations discussed in this paper on Pentium Pro computers.

The side walls and bottom of the container are impenetrable, and ball-wall collisions are taken to have the same values of ϵ, μ, and β_0 as ball-ball collisions. The side walls in the simulation are stationary, while in the experiment the side walls are rigidly attached to the oscillating bottom of the container.

We determine ϵ by comparing wavelengths λ determined from simulations and experiments at a single set of parameter values: $\Gamma = 3.0$, $f^* = 0.205$, and $N = 2.71$. (For these parameter values we cannot discern any dependence of λ on μ.) An increase of ϵ from 0.5 to 0.8 produces a 30% decrease in the wavelength. The value of ϵ determined in this way, 0.7, is then used in all the simulations. This ϵ value is larger than measured values of the restitution coefficient for lead [8], but model collisions are instantaneous and hence binary, while experimental collision durations are finite. In the experiment, as particles collide with the plate, energy dissipates until many of the particles are in contact and the plate lifts the layer as a body. Thus, many more collisions are simulated than

experimentally occur. To preserve the total dissipation in the simulations, a smaller number of more inelastic collisions are modeled with a larger number of less inelastic collisions.

With ϵ in hand, we examine the dependence of λ on μ at another point in parameter space, $\Gamma = 3.0$, $f^* = 0.534$, and $N = 5.42$. We find that λ is nearly constant for μ equal to $0.25, 0.5$, and 0.75, but for $\mu = 0$, λ is decreased by nearly 25%. This suggests that rotations, excited through dissipative tangential contacts, increase the horizontal mobility of the particles. Based on these investigations, we set $\mu = 0.5$. The values $\epsilon = 0.7$ and $\mu = 0.5$, derived from only the two points in the parameter space (Γ, f^*, N), are used for *all* simulations presented here.

Wavelengths.—Figure 2 presents our results for the dimensionless wavelength $\lambda^* = \lambda/H$ as a function of f^*. Scaling in this way collapses these data. The results from our simulations and experiments are in good quantitative agreement, even showing the same change in behavior at $f^* \approx 0.5$. These data are also consistent with previously reported experimental data [2]. To test the dependence of λ^* on aspect ratio, experiments were also conducted with bronze spheres for which $D = 0.165$ mm and $L/D = 982$. At $L/D = 100$, the container walls influence the orientation of the observed patterns, and there is a tendency for peaks of the wave to exist at the walls [e.g., see Fig. 1(a)]. However, the wavelengths measured for the two aspect ratios are in agreement, differing only for wavelengths larger than one half of the container length. Note that the kink at $f^* \approx 0.5$ appears also for the larger aspect ratio.

Transitions.—Figure 3 shows the regions in the Γ-f^* plane in which various spatial patterns occur. This diagram, obtained for 0.55 mm lead particles (with $N = 5.42$ and $L/D = 100$) is in good accord with the diagram in [3], obtained for 0.165 mm bronze particles (with $N = 7.3$ and $L/D = 770$). This agreement, as well as that for the wavelengths for lead and bronze particles shown in Fig. 2, indicates that the patterns are rather insensitive to particle properties.

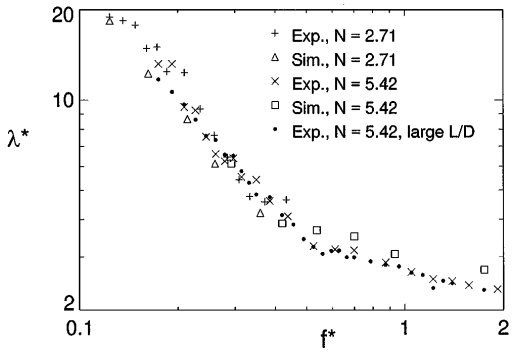

FIG. 2. Wavelength vs frequency from simulations and experiments with $\Gamma = 3.0$. The + and × points are obtained from experiments with lead spheres ($D = 0.55$ mm) and $L/D = 100$, while the • points correspond to experiments with bronze spheres ($D = 0.165$ mm) and $L/D = 982$.

When the acceleration amplitude of the cell is increased above g, the granular layer leaves the supporting plate for part of each cycle, but the layer remains flat until a critical acceleration Γ_c is reached; for $\Gamma > \Gamma_c$, square [Fig. 1(a)] or stripe [Fig. 1(b)] standing wave patterns spontaneously form. At higher Γ, both types of patterns become unstable to hexagons [Figs. 1(c) and 1(d)]. As Γ is further increased, the layer begins to collide with the plate on only every other plate oscillation, and the flat state is recovered [Fig. 1(e)]. At a higher acceleration $\Gamma_{c,2}$, the flat layer again bifurcates to squares [Fig. 1(f)] or stripes [Fig. 1(g)], now oscillating at $f/4$. These patterns become unstable to $f/4$ hexagons [Fig. 1(h)] at still higher Γ.

We now exploit observations from the simulations to develop a heuristic argument for the value of the critical acceleration for the onset of patterns Γ_c. One period T of the plate's oscillation may be broken up into two disjoint parts. During the time interval t_d between the collision of the layer with the plate and the apogee of the layer's bottom, peaks of the pattern decay. The layer becomes flat just before (about 5% of the pattern period before) the bottom particles reach their apogee. Then peaks grow during the time interval t_g between the apogee and the next collision with the plate. Finally, we observe that for square and stripe patterns, $t_g = t_d = T/2$; i.e., the layer bottom's apogee occurs halfway between collisions with the plate; see Fig. 4.

We conjecture that states without patterns correspond to $t_d > t_g$; patterns decay during the extra time spent in

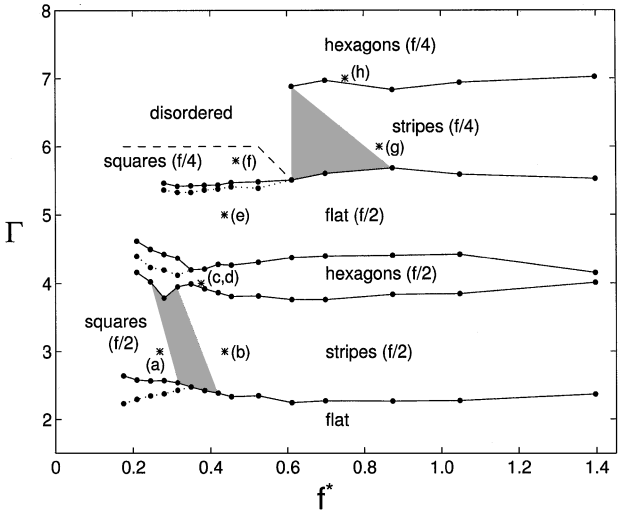

FIG. 3. Phase diagram obtained in the experiments. The parameter values for the comparison in Fig. 1 of patterns from the simulations and experiments are indicated by (a) through (h). The transitions from a flat layer to square patterns are hysteretic: solid lines denote the transition for increasing Γ, while dotted lines denote it for denote decreasing Γ. Shaded areas show transitional regions between stripes and squares.

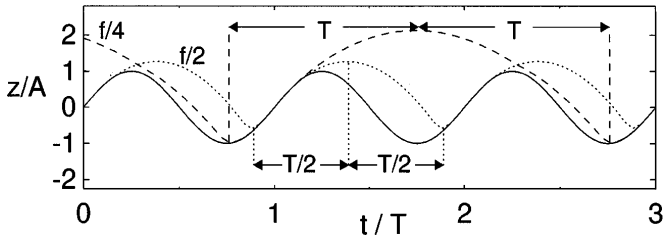

FIG. 4. Trajectories of the layer bottom from simulations. The $f/2$ and $f/4$ curves are obtained at points (a) and (g) on Fig. 3, and the solid line shows the motion of the plate.

the damping part of the cycle. If the collision between plate and layer occurred while the plate was descending, the apogee of the layer bottom could not occur before the plate reached its maximum height, at a time greater than $T/2$ after the collision. Since $t_d > T/2$ and $t_d + t_g = T$, we find that $t_d > t_g$ and we suppose that patterns will not be stable. Hence, the marginal trajectory for pattern stability is one for which the collision occurs at the plate's lowest point and the layer bottom's apogee occurs at the plate's highest location. This layer free falls from its apogee through a distance $2A$ to collide with the plate bottom after a time $T/2$, so that $2A = gT^2/8$ or $\Gamma_c = (2\pi)^2/16 \approx 2.47$, in accord with experiment (Fig. 3).

We observe that the crossover between stripes and squares occurs when the distance vertically traversed by the layer bottom from apogee to collision, $gT^2/8$, equals the depth of the layer H so that the frequency of the square-stripe transition is given by $f^*_{ss} = 1/\sqrt{8} \approx 0.35$ (cf. Fig. 3). Unlike the kink in Fig. 2, f^*_{ss} has been found to be independent of N [7].

For $f/4$ patterns, the behavior is the same as that of their $f/2$ counterparts: growth of peaks between apogee and collision, decay of peaks between collision and apogee, and temporal centering of the apogee between consecutive collisions, which in this case are separated by $2T$; see Fig. 4. We suppose that the marginal trajectory in this case is one in which the layer bottom's apogee occurs when the plate is at its lowest point; an earlier apogee will not allow the collisions to occur on only every other plate oscillation. Simulation shows that for this trajectory, the bottom of the layer reaches a height of about $3.4A$, so that $3.4A = gT^2/2$, or $\Gamma_{c,2} = (2\pi)^2/6.8 \approx 5.81$, in accord with experiment (Fig. 3). We also observe that, once again, the square-stripe transition corresponds to the frequency at which the distance traveled from apogee to collision, $gT^2/2$, equals the depth of the layer H, or $f^*_{ss,2} = 1/\sqrt{2} \approx 0.71$.

The present work validates our model, which can now be used to examine many outstanding issues in vibrated granular media, such as the variation of particle transport properties with frequency and acceleration. The simulations can be used to determine coefficients in phenomenological models proposed to describe granular patterns (e.g., [4]). Also, through appropriate spatial averaging it may be possible to construct continuum equations and subject them to standard stability analyses to gain insight into the pattern formation processes.

We thank Paul Umbanhowar for many valuable suggestions and Joe Newman for writing our original event driven code. This research is supported by the Department of Energy Office of Basic Energy Sciences and the Texas Advanced Research Program.

*Electronic address: bizon@chaos.ph.utexas.edu
†Electronic address: swinney@chaos.ph.utexas.edu

[1] M. C. Cross and P. C. Hohenberg, Rev. Mod. Phys. **65**, 851 (1993).
[2] F. Melo, P. Umbanhowar, and H. L. Swinney, Phys. Rev. Lett. **72**, 172 (1994); P. Umbanhowar, F. Melo, and H. L. Swinney, Nature (London) **382**, 793 (1996); E. Clément, L. Vanel, J. Rajchenbach, and J. Duran, Phys. Rev. E **53**, 2972 (1996).
[3] F. Melo, P. B. Umbanhowar, and H. L. Swinney, Phys. Rev. Lett. **75**, 3838 (1995).
[4] L. Tsimring and I. Aranson, Phys. Rev. Lett. **79**, 213 (1997); T. Shinbrot, Nature (London) **389**, 574 (1997); D. H. Rothman (to be published).
[5] K. M. Aoki and T. Akiyama, Phys. Rev. Lett. **77**, 4166 (1996); D. C. Rapaport, Physica A (to be published).
[6] S. Luding, E. Clément, J. Rajchenbach, and J. Duran, Europhys. Lett. **36**, 247 (1996).
[7] P. B. Umbanhowar, F. Melo, and H. L. Swinney (to be published).
[8] W. Goldsmith, *Impact* (Edward Arnold Ltd., London, 1960), pp. 257–267.
[9] S. McNamara and W. R. Young, Phys. Fluids A **4**, 496 (1992).
[10] O. R. Walton, in *Particulate Two-Phase Flow*, edited by M. C. Roco (Butterworth-Heinemann, Boston, 1993), pp. 884.
[11] T. G. Drake, Ph.D. thesis, UCLA, 1988; N. Maw, J. R. Barber, and J. N. Fawcett, Wear **38**, 101 (1976); Trans. ASME, J. Lub. Tech. **20**, 327 (1981).
[12] D. C. Rapaport, J. Comput. Phys. **34**, 184 (1980).
[13] B. D. Lubachevsky, J. Comput. Phys. **94**, 255 (1991); M. Marín, D. Risso, and P. Cordero, J. Comput. Phys. **109**, 306 (1993).